General Disclaimer

One or more of the Following Statements may affect this Document

- This document has been reproduced from the best copy furnished by the organizational source. It is being released in the interest of making available as much information as possible.

- This document may contain data, which exceeds the sheet parameters. It was furnished in this condition by the organizational source and is the best copy available.

- This document may contain tone-on-tone or color graphs, charts and/or pictures, which have been reproduced in black and white.

- This document is paginated as submitted by the original source.

- Portions of this document are not fully legible due to the historical nature of some of the material. However, it is the best reproduction available from the original submission.

Produced by the NASA Center for Aerospace Information (CASI)

(NASA-CR-158103) DATA ACQUISITION AND PATH SELECTION DECISION MAKING FOR AN AUTONOMOUS ROVING VEHICLE Progress Report, 1 Jan. 1978 - 31 Dec. 1978 (Rensselaer Polytechnic Inst., Troy, N. Y.) 35 p HC A03/MF A01 G3/14 N79-16890 Unclas 13966

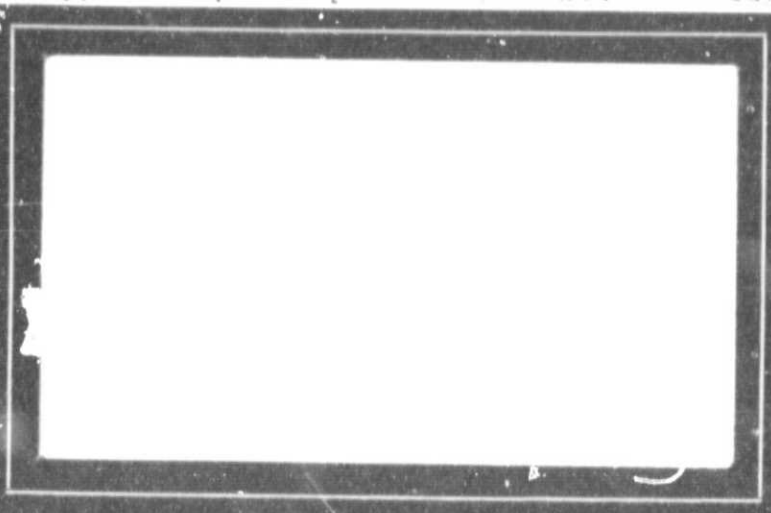

Rensselaer Polytechnic Institute

Troy, New York 12181

RPI TECHNICAL REPORT MP-62

PROGRESS REPORT FOR
January 1, 1978 to December 31, 1978

DATA ACQUISITION AND PATH SELECTION DECISION MAKING FOR AN AUTONOMOUS ROVING VEHICLE

NATIONAL AERONAUTICS
and
SPACE ADMINISTRATION
GRANT NGL 7184
NSG

C. N. Shen

S. W. Yerazunis

RENSSELAER POLYTECHNIC INSTITUTE
TROY, NEW YORK

January 1979

TABLE OF CONTENTS

ABSTRACT

The feasibility of using range/pointing angle data such as might be obtained by a laser rangefinder for the purpose of terrain evaluation in the 10-40 meter range on which to base the guidance of an autonomous rover has been further investigated. The decision procedure of the Rapid Estimation Scheme for the detection of discrete obstacles has been modified to reinforce the detection ability. With the introduction of the logarithmic scanning scheme and obstacle identification scheme, previously developed algorithms are combined to demonstrate the overall performance of the integrated route designation system using laser rangefinder. In an attempt to cover a greater range, 30m to 100m, the problem estimating gradients in the presence of positioning angle noise at middle range is investigated.

DATA ACQUISITION AND PATH SELECTION DECISION MAKING FOR AN AUTONOMOUS ROVING VEHICLE

I. INTRODUCTION

Current national goals now include an autonomous rover mission to Mars in 1986 and a possible sample return mission for Mars in 1990. The values to be derived from these missions will depend on the extent of the ranges of exploration which are permitted by the roving devices and the effectiveness of their guidance systems.

The large round-trip communications delay which ranges from about nine to forty-five minutes, depending on the positions of Mars and Earth, precludes direct earth control except for emergency situations. Systems capable of sensing terrain, detecting hazards and selecting safe but efficient paths towards desired locations are essential.

In seeking alternative concepts for the unmanned exploration of Mars, consideration should be given to: (a) the character of the rover, and (b) the path selection system.

The mobility, maneuverability and stability of the rover will have a direct influence on the availability of safe paths to the desired locations. A rover of limited ability to handle in-path or cross-path slopes or boulders, craters, trenches, etc., will be forced to follow tortuous paths to the specified destinations. Indeed if its mobility is sufficiently limited, there may in many cases be no acceptable path. Thus, one objective of research and development programs should be the conception and evaluation of rovers of exceptional mobility.

The quality of the path selection systems which are available will also have a profound influence on the mission. The term "path selection system" is intended to encompass the devices employed to gather terrain information, the procedures by which these data are processed and the algorithms used to select the optimal path. A path selection system possessing a poor capability to discriminate between safe and hazardous features will have to be biased conservatively to protect the rover. In such a case, an unnecessarily longer path will have to be followed. Indeed, in certain situations, the conservative bias may exclude all possible paths and segments of the mission will go unfulfilled. On the other hand, a path selection system of high accuracy and perceptiveness will make it possible to take full advantage of the mobility of the rover. Shorter paths will be followed, less time will be consumed and more areas will be explored.

Research programs at Rensselaer have been aimed at both of these major objectives. The research program described herein has been focused on the feasibility of using range/pointing angle data, such as might be acquired by a laser rangefinder, to characterize the terrain in such detail as required for safe designation of route for an autonomous rover and on the development of path selection algorithms employing such information.

II. SUMMARY OF PROGRESS

The research program during the past year addressed the following topics:

1. Middle range gradient estimation with noisy elevation angle.

2. Obstacle detection by rapid estimation scheme with modified decision tree.

3. Integrated path selection system utilizing obstacle detection and terrain modeling algorithms.

First, an approach to the problem of estimating in-path and cross-path slopes in the presence of positioning angle noises at middle range, 30m to 100m, has been developed. The change in slopes has been expressed as a function of the noise perturbations affecting the elevation angle measurements.

Second, decision procedure of the Rapid Estimation Scheme and the evaluation of the probabilities are modified to reinforce the detection ability. Simulation results show that the modified version succeeded in reducing almost all the false detections at far distances. Also, it showed increased detection ability at near distances.

Third, with the introduction of logarithmic scanning scheme, and obstacle identification scheme, an overall performance of the integrated path selection system is demonstrated. This integral path selection system defines the coordinations among the previously developed algorithms such as Rapid Estimation Scheme, terrain modeling, and path selection algorithms. The computer simulation results are promising in that the rover is capable of electing a locally optimum path for low risk and energy expenditure while maintaining a desired target direction.

III. DETAILED PROGRESS REVIEW

TASK A. Gradient Estimation at Middle Range - Ricardo Mediavilla

Faculty Advisor: Prof. C. N. Shen

1) Genesis of the problem - Stochastically Spaced Rows of a Measurement Matrix.

The middle range, some 30 to 100 meters distance, poses a problem for Mars rover navigation. If a laser rangefinder is located at the top of the mast of the rover, say two meters above the ground, a horizontal terrain point 100 meters away has a very shallow elevation angle of about 0.02 radians. A point 2 meters inward from the first point (98 meters from the laser mast) will have an elevation angle β of 0.0204 radians, which makes an included angle $\Delta\beta$ of 0.0004 radians, or about 1.5 arc-minutes. This approaches the standard deviation of the measurement of the elevation angle $\delta\beta$, which at present can be assumed to be 1 arc-minute. In this case the rows of the range matrix displace stochastically.

2) Introduction.

Terrain iso-gradients can be used to evaluate passable terrain regions

for an unmanned roving vehicle to be used on Mars' surface. Range data, measured in a spherical coordinate system, is stored in a range matrix. Such range matrix consist of a listing of the distance measurements from a ranging device to the terrain surface as a function of azimuth and elevation angle measurements. So far, the range data matrix has been assumed to be fixed in spacing since the noise in the elevation and azimuth directions is small. However, for the shallow elevation angles near the skyline the magnitude of the noise in the elevation angle can approach that of the signal, displacing the information in the range data matrix.

3) Scanning scheme

Range data are stored in the range matrix

$$[r] = \begin{bmatrix} r_{11} & r_{12} & \cdot & \cdot & \cdot & r_{1n} \\ r_{21} & r_{22} & \cdot & \cdot & \cdot & \\ \cdot & \cdot & r_{i-1j} & & & \\ \cdot & \cdot & r_{ij} & r_{i+1j} & & \\ & r_{i-1j} & r_{i+1j} & & & \\ & & r_{i+1j} & & & \\ r & & & & & r_{mn} \end{bmatrix}$$

where β, the elevation angle, varies with index i, and θ, the azimuth angle, varies with index j.

In order to change the data spacing as a linear function of the radial distance ρ_i from the rover it is desired that $\Delta\rho_i = \rho_i \Delta\theta$. (See Figs. 1-a and 1-b.)

$$\Delta\rho_i = \rho_i \Delta\theta \tag{1}$$

$$\tan\beta_{i+1} = \frac{H}{\rho_{i+1}} = \frac{H}{\rho_i - \Delta\rho_i}$$

$$\tan\beta_{i+1} = \frac{H}{\rho_i - \rho_i \Delta\theta}$$

$$\rho_i \tan\beta_{i+1} = \frac{H}{1-\Delta\theta}$$

$$\rho_i \Delta\theta \tan\beta_{i+1} = \frac{H\Delta\theta}{1-\Delta\theta}$$

Thus, a recursive equation for the calculation of β_{i+1} is given by

$$\Delta\rho_i \tan\beta_{i+1} = \frac{H\Delta\theta}{1-\Delta\theta} \tag{2}$$

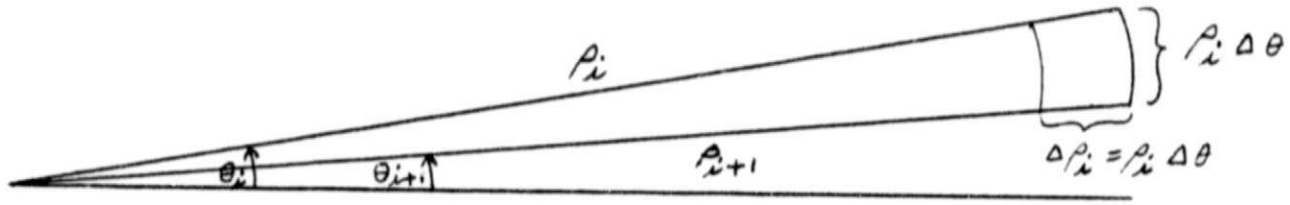

Fig. 1-a. Horizontal Projection of Range Measurement.

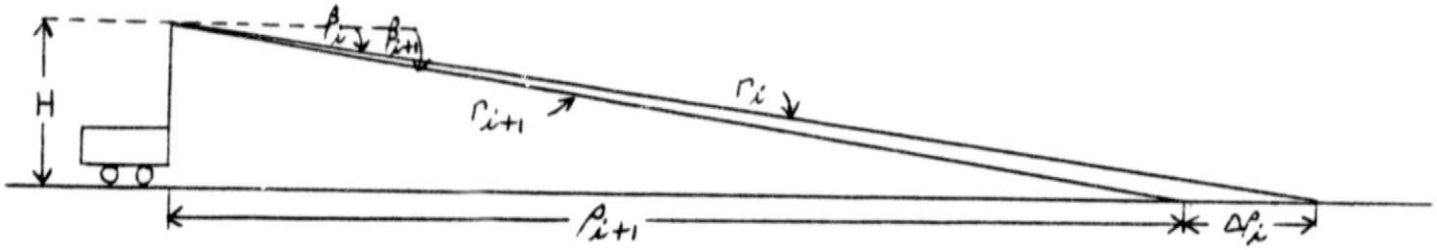

Fig. 1-b. Range Measurement.

4) Computation of row spacing.

Taking $\Delta\theta$ as constant in equation (2), the elevation angle β_i is recursively calculated. Table I shows some typical calculations of the elevation angle β_i where equation (2) and a value of $\Delta\theta$ = .03 radians has been used.

Note that as the distance from the rover becomes smaller, $\Delta\beta$>>1 arc-minute, and the error $\delta\beta$ in elevation angle measurement becomes negligible compared to $\Delta\beta$, the angle increment.

Table I

Recursive Calculation of Elevation Angle β for Horizontal Terrain

Elevation Angle β (radians)	Distance from Mars Rover ρ (meters)	$\Delta\rho$ (meters)	$\Delta\beta$ (radians)	$\Delta\beta$ (arc-minutes)
.02499	92.11	1.53	.00078	2.69
.02577	90.58			
.02910	83.28	2.48	.00090	3.11
.03000	80.80			
.05687	30.98	.64	.00175	6.03
.05862	30.34			
.15485	13.45	.40	.00475	16.32
.15960	13.05			

5) Error in slope due to error in elevation angle measurement.

Fig. 2 shows that at far distances from the rover the error in the elevation angle measurement can seriously offset the slope calculation.

Let $\delta\beta$ represent the error in the elevation angle measurement. The following quantities are assumed to be:

$$\rho_i = 100 \text{ meters} \qquad H = 2 \text{ meters}$$

$$\delta\beta = 1 \text{ arc-minute}$$

Then from Fig. 2 we have

$$\tilde{r}_i = \frac{H}{\sin(\beta_i + \delta\beta)} = 98.586$$

and

$$\tilde{r}_{i+1} = \frac{H}{\sin(\beta_{i+1} - \delta\beta)}$$

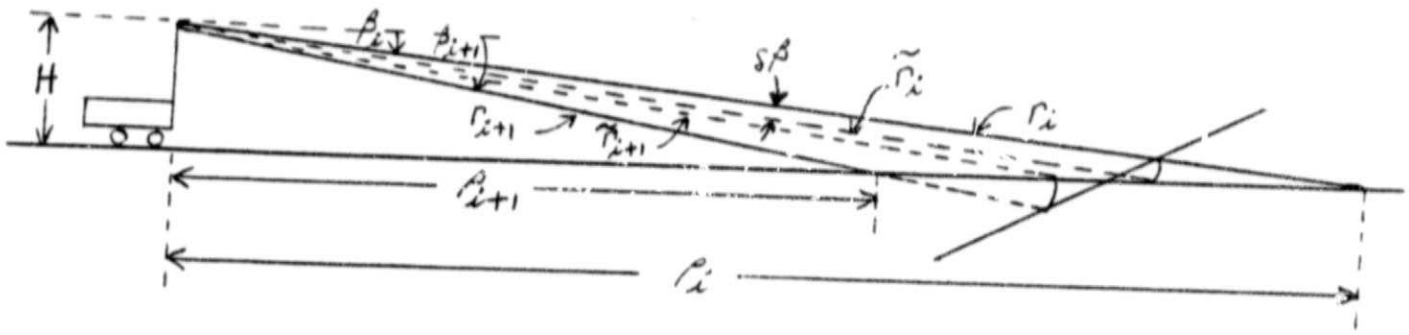

Fig. 2. Noise Effect in the Calculation of In-Path Slope at 100 Meters.

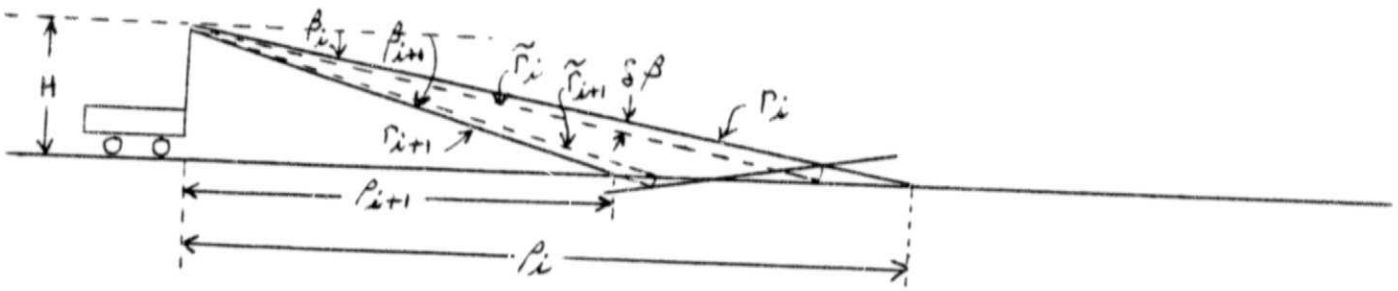

Fig. 3. Noise Effect in the Calculation of In-Path Slope at 30 Meters.

where β_{i+1} has been calculated using equation (2). The terrain slope is given by

$$\text{slope} = -\frac{\tilde{r}_{i+1}\sin\beta_{i+1} - \tilde{r}_i\sin\beta_i}{\tilde{r}_{i+1}\cos\beta_{i+1} - \tilde{r}_i\cos\beta_i} \tag{3}$$

Fig. 3 shows that at a distance of 30 meters from the rover the error in the elevation angle measurement does not have as serious an effect as in the case of 100 meters distance. Let

$$\rho_i = 30 \text{ meters} \qquad H = 2 \text{ meters}$$

$$\delta\beta = 1 \text{ arc-minute}$$

$$\tilde{r}_i = \frac{H}{\sin(\beta_i + \delta\beta_i)} = 29.936$$

$$\tilde{r}_{i+1} = \frac{H}{\sin(\beta_{i+1} - \delta\beta)} = 29.292$$

Using equation (3), it is obtained

$$\text{slope} = .026$$

In a flat terrain condition an error of 1 arc-minute in the elevation angle measurement will produce an in-path slope of .323 when the distance from the rover is 100 meters, and an in-path slope of only .026 when the distance from the rover is 30 meters.

6) Evaluation of the in-path slopes from range slopes.

So far the approach that has been followed is that of recursively estimating the range slopes in spherical coordinates, and then transforming to a cylindrical coordinate system to obtain the terrain slopes. As seen from Fig. 4 the equations describing the coordinate transformation are given by

$$\rho_{ij} = r_{ij}\cos\beta_{ij} \tag{4}$$

$$\theta_{ij} = \theta_{ij} \tag{5}$$

$$Z_{ij} = H - r_{ij}\sin\beta_{ij} \tag{6}$$

Taking differentials of equations (4) and (6) one obtains

$$dZ = \frac{\partial Z}{\partial \beta} \cdot d\beta + \frac{\partial Z}{\partial r}\, dr \tag{7}$$

$$d\rho = \frac{\partial \rho}{\partial \beta} \cdot d\beta + \frac{\partial \rho}{\partial r}\, dr \tag{8}$$

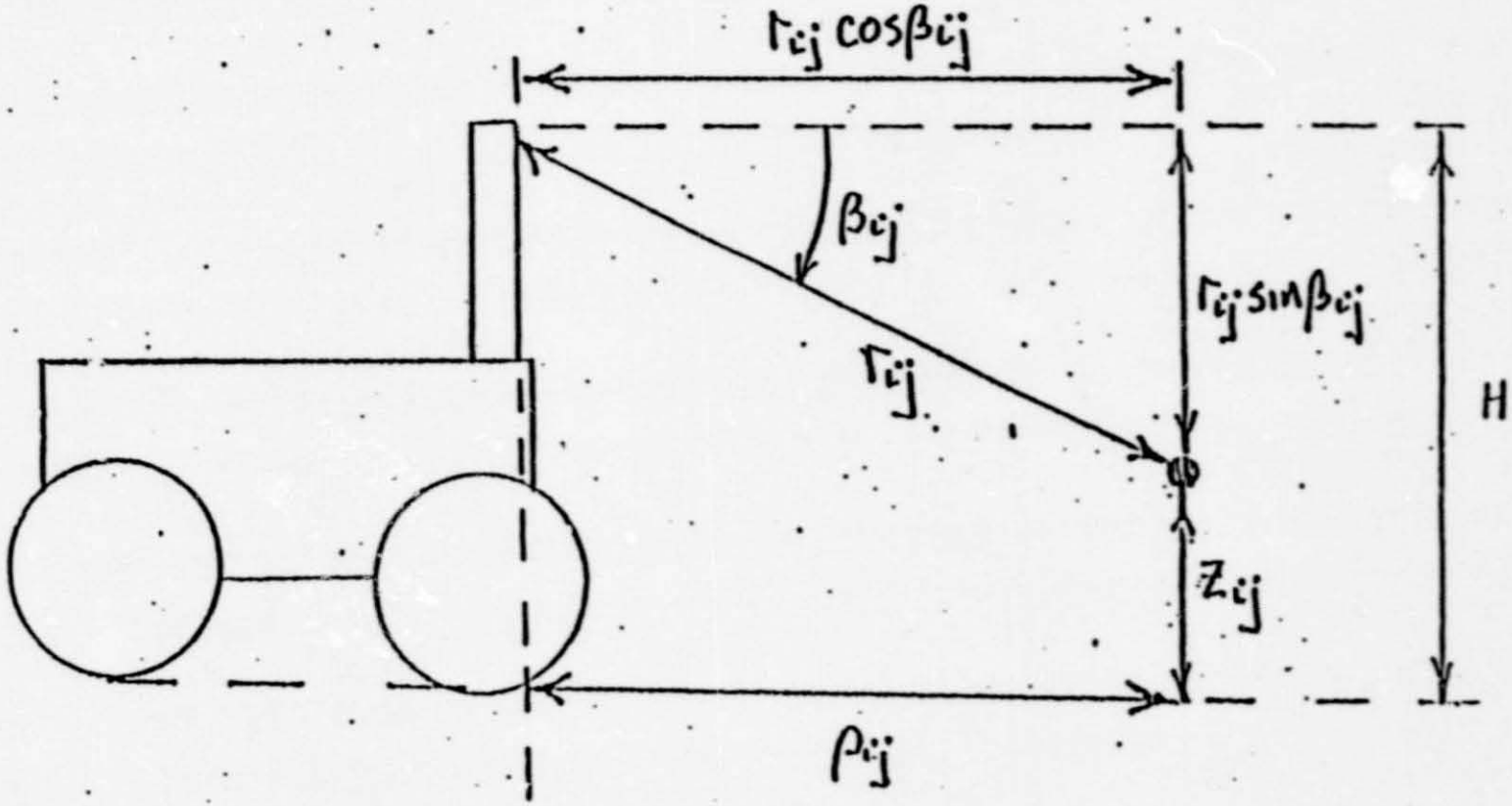

Figure 4. Relationship between spherical and cylindrical coordinate systems

The in-path terrain slope becomes

$$\frac{dZ}{d\rho} = \frac{dz/d\beta}{d\rho/d\beta} = \frac{\frac{\partial Z}{\partial \beta} + \frac{\partial Z}{\partial r} \cdot \frac{dr}{d\beta}}{\frac{\partial \rho}{\partial \beta} + \frac{\partial \rho}{\partial r} \cdot \frac{dr}{d\beta}} \tag{9}$$

where $dr/d\beta$ is the in-path range slope.

7) Evaluation of the in-path slopes in terms of the inverse of the range slopes.

At middle range the error in the elevation angle measurement $\delta\beta$ cannot be neglected. (See Fig. 5.)

Let $\hat{r}_i$ and $\hat{r}_{i+1}$ be the best available estimates of the range measurements. Define

$$\Delta\rho_i = \rho_i - \rho_{i+1} \qquad \Delta\beta = \beta_{i+1} - \beta_i \tag{10}$$

$$\Delta Z = Z_i - Z_{i+1} \qquad -\Delta\beta = \beta_i - \beta_{i+1} \tag{11}$$

$$\Delta\hat{r} = \hat{r}_i - \hat{r}_{i+1} \tag{12}$$

As before, the spherical to cylindrical coordinate transformation equations are given by:

$$\rho = \hat{r}\cos\beta \tag{13}$$

$$\theta = \theta \tag{14}$$

$$Z = H - \hat{r} \tag{15}$$

Taking differentials of equations (13) and (15) one obtains

$$dZ = \frac{\partial Z}{\partial \beta} d\beta + \frac{\partial Z}{\partial \hat{r}} d\hat{r} \tag{16}$$

$$d\rho = \frac{\partial \rho}{\partial \beta} d\beta + \frac{\partial \beta}{\partial \hat{r}} d\hat{r} \tag{17}$$

Assuming that the error in the range measurement $\hat{r}$ has a standard deviation of 5 centimeters, its effect can be neglected as compared to the effect of error in the elevation angle measurement β. So, this time derivatives are taken with respect to r.

$$\frac{dZ}{d\rho} = \frac{dZ/d\hat{r}}{d\rho/d\hat{r}} = \frac{\frac{\partial Z}{\partial \beta}\frac{d\beta}{d\hat{r}} + \frac{\partial Z}{\partial \hat{r}}}{\frac{\partial \rho}{\partial \beta}\frac{\partial \beta}{\partial \hat{r}} + \frac{\partial \rho}{\partial \hat{r}}} \tag{18}$$

Comparing equation (18) with equation (9) one can see that in equation (18) r is considered known while β is stochastic. In equation (9) the

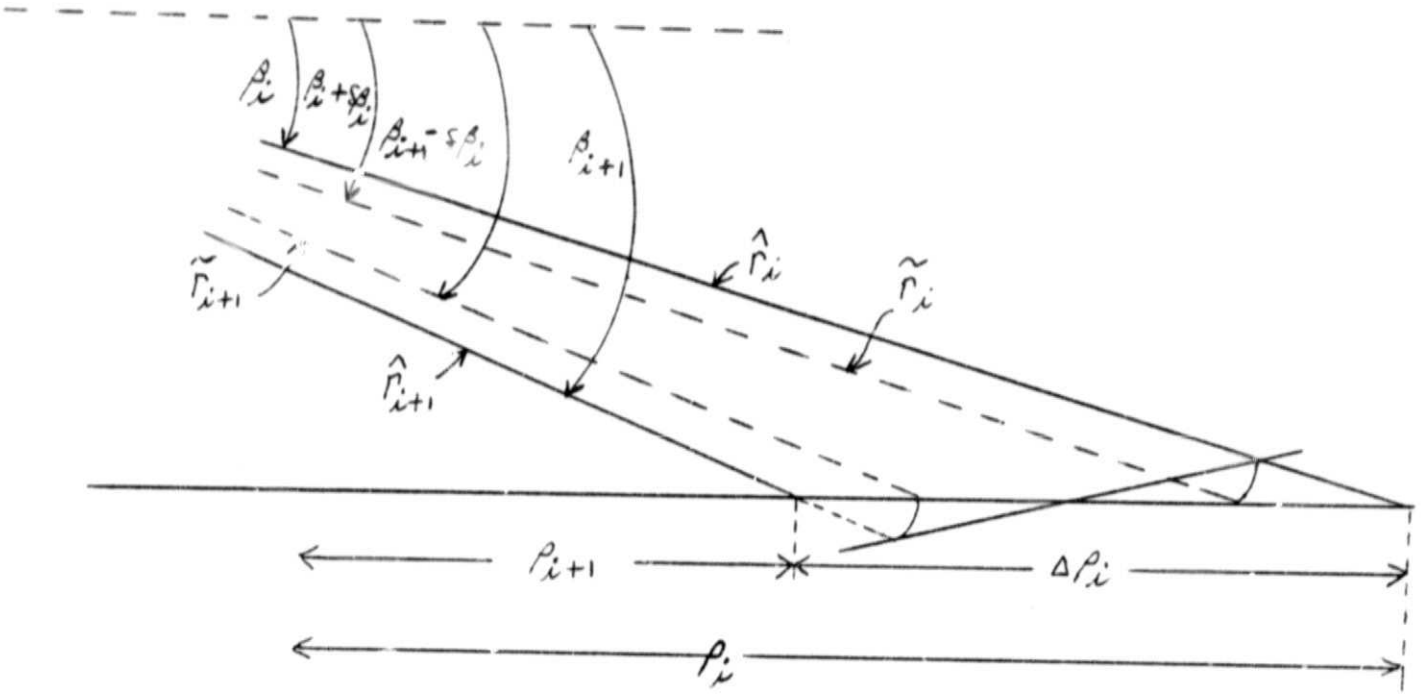

Fig. 5. Displacements in the Range Measurements Caused by Noise in the Elevation Angle Measurement.

error in β is negligible, and so β is considered to be fixed. For these reasons differentials are taken with respect to β in equation (9) and with respect to $\hat{r}$ in equation (18).

From the spherical to cylindrical transformation equations, (13) through (15), one obtains:

$$\frac{\partial Z}{\partial \beta} = -\hat{r}\cos\beta \qquad \frac{\partial \rho}{\partial \hat{r}} = \cos\beta$$

$$\frac{\partial Z}{\partial \hat{r}} = -\sin\beta \qquad \frac{\partial \rho}{\partial \beta} = -\hat{r}\sin\beta$$

$$\text{in-path slope} = \frac{dZ}{d\rho} = \frac{(-\hat{r}\cos\beta)\,\frac{d\beta}{d\hat{r}} - \sin\beta}{(-\hat{r}\sin\beta)\,\frac{d\beta}{d\hat{r}} + \cos\beta} = \frac{-\hat{r}\,\frac{d\beta}{d\hat{r}} - \tan\beta}{-\hat{r}(\tan\beta)\,\frac{d\beta}{d\hat{r}} + 1} \tag{19}$$

where $\frac{d\beta}{d\hat{r}}$ is the inverse of the range slope.

Let $\tan\gamma = -\hat{r}\,\frac{d\beta}{d\hat{r}}$. Then

$$\frac{dZ}{d\rho} = \frac{\tan\gamma - \tan\beta}{1 + \tan\gamma\tan\beta} = \tan(\gamma-\beta) \tag{20}$$

When $\Delta\hat{r} \to 0$ in equation (20) the terrain will be interpreted as a vertical wall and $\tan\gamma \to \infty$, creating a problem in the evaluation of $dZ/d\rho$.

8) Error analysis.

Fig. 5 shows how noise $\delta\beta$ in the elevation angle measurement β can displace the range measurement r. Let $\hat{r}$ represent the actual range measurement after accounting for the noise in the β measurement. Let $\delta\beta_i$ be Gaussian random noise of zero mean and 1 arc-minute standard deviation. An expression will be derived relating a change in slope due to $\delta\beta$.

$$\tilde{r}_{i+1} = \frac{H}{\sin(\beta_{i+1} - \delta\beta_{i+1})}$$

$$\tilde{r}_i = \frac{H}{\sin(\beta_i + \delta\beta_i)}$$

$$y_{i+1} = \tilde{r}_{i+1}\sin\beta_{i+1} = \frac{H\sin\beta_{i+1}}{\sin(\beta_{i+1} - \delta\beta_{i+1})}$$

$$x_{i+1} = \tilde{r}_{i+1}\cos\beta_{i+1} = \frac{H\cos\beta_{i+1}}{\sin(\beta_{i+1} - \delta\beta_{i+1})}$$

$$y_i = \tilde{r}_i \sin\beta_i = \frac{H\sin\beta_i}{\sin(\beta_i + \delta\beta_i)}$$

$$x_i = \tilde{r}_i \cos\beta_i = \frac{H\cos\beta_i}{\sin(\beta_i + \delta\beta_i)}$$

Define δS as the change in slope due to a perturbation in β_i and β_{i+1}

$$\delta S = -\frac{y_{i+1} - y_i}{x_{i+1} - x_i} \tag{21}$$

$$= -\frac{\sin\beta_{i+1}\sin(\beta_i + \delta\beta_i) - \sin\beta_i\sin(\beta_{i+1} - \delta\beta_{i+1})}{\cos\beta_{i+1}\sin(\beta_i + \delta\beta_i) - \cos\beta_i\sin(\beta_{i+1} - \delta\beta_{i+1})}$$

$$= -\frac{\sin\beta_{i+1}[\sin\beta_i\cos\delta\beta_i + \cos\beta_i\sin\delta\beta_i] - \sin\beta_i[\sin\beta_{i+1}\cos\delta\beta_{i+1} - \cos\beta_{i+1}\sin\delta\beta_{i+1}]}{\cos\beta_{i+1}[\sin\beta_i\cos\delta\beta_i + \cos\beta_i\sin\delta\beta_i] - \cos\beta_i[\sin\beta_{i+1}\cos\delta\beta_{i+1} - \cos\beta_{i+1}\sin\delta\beta_{i+1}]} \tag{22}$$

Since $\delta\beta$ is small, the following approximations can be used:

$$\cos\delta\beta_i = 1 \tag{23}$$

$$\cos\delta\beta_{i+1} = 1 \tag{24}$$

$$\sin\delta\beta_i = \delta\beta_i \tag{25}$$

$$\sin\delta\beta_{i+1} = \delta\beta_{i+1} \tag{26}$$

Approximations (23) through (26) are valid since $\delta\beta_i$ is Gaussian with zero mean and 1 arc-minute standard deviation.

$$\delta S \approx -\frac{\sin\beta_{i+1}[\sin\beta_i + \delta\beta_i\cos\beta_i] - \sin\beta_i[\sin\beta_{i+1} - \delta\beta_{i+1}\cos\beta_{i+1}]}{\cos\beta_{i+1}[\sin\beta_i + \delta\beta_i\cos\beta_i] - \cos\beta_i[\sin\beta_{i+1} - \delta\beta_{i+1}\cos\beta_{i+1}]}$$

$$\delta S \approx -\frac{\delta\beta_i\tan\beta_{i+1} + \delta\beta_{i+1}\tan\beta_i}{\tan\beta_i - \tan\beta_{i+1} + \delta\beta_i + \delta\beta_{i+1}} \tag{27}$$

If it is also assumed that $\delta\beta = \delta\beta_{i+1}$ then equation (26) becomes

$$\delta S \approx \frac{\delta\beta_i(\tan\beta_i + \tan\beta_{i+1})}{(\tan\beta_{i+1} - \tan\beta_i) - 2\delta\beta_i} \tag{28}$$

From equation (10) it is obtained that

$$\tan\beta_{i+1} = \tan(\beta_i + \Delta\beta) = \frac{\tan\beta_i + \tan\Delta\beta}{1 - \tan\beta_i\tan\Delta\beta} \tag{29}$$

If β_{i+1} and β_i are both small, then

$$1 - \tan\beta_i \tan\Delta\beta \to 1 \text{ and}$$

equation (29) becomes

$$\tan\beta_{i+1} \approx \tan\beta_i + \tan\Delta\beta$$

$$\delta S \approx (\tan\beta_i + \tan\beta_{i+1}) \frac{\delta\beta_i}{(\tan\Delta\beta) - 2\delta\beta_i}$$

$$\delta S \approx \left(\frac{\tan\beta_i + \tan\beta_{i+1}}{2}\right) \frac{\left(\frac{2}{\tan\Delta\beta}\right)\delta\beta_i}{1 - \left(\frac{2}{\tan\Delta\beta}\right)\delta\beta_i}$$

Some method of analysis should be developed for obtaining the variance of δS if $\delta\beta_i$ is Gaussian.

TASK B. Obstacle Detection by Stabilized Rapid Estimation Scheme with Modified Detection Tree - C. S. Kim
Faculty Advisor: Prof. C. N. Shen

Rapid Estimation Scheme, Reference 1, was developed earlier to detect the outlines of discrete obstacles by processing noisy contaminated range measurement data obtained from laser rangefinder. It was found that the system equations of the previous R.E.S. are unstable, since the eigenvalues of the system matrix lie outside of unit circle in the 8-plane. For the reason above, the previous R.E.S. generated many false detections in identifying the outlines of the obstacles at the ranges greater than 30m or less than 10m. A stable system model was formulated by introducing weighting parameters and reversing the direction of the recursive estimation and detection procedure. As a result, increasing accuracy in state estimates reduced the number of false detections. It was reported, Reference 9, that the stabilized R.E.S. succeeded in detecting the complete outlines of obstacles at 40m away from the rover. However, it was also pointed out that the conditional probabilities following the input estimation were evaluated by approximation. Thus, the effect of the approximation was partially compensated by assigning excessive penalties to false detections in the Bayes decision process. For the reason above, the detection ability of the scheme is weakened and the R.S.E. was not able to detect an input whose signal to noise ratio is less than 4.5.

In an effort to increase the detection ability of the R.E.S., modifications have been made to the structure of the decision process and the input estimation process. Simulation results show that this modified R.E.S. generates only few false detections in identifying the complete outlines of obstacles at 40m without assigning excessive penalties to false detections. Also, the modified R.E.S. detected half of the bottom edges of the boulder at 4m where the signal to noise ratio is in the neighborhood of 1.5. The following describes modifications made to the decision process and input estimation procedure:

R.E.S. estimates the state of the system by using an input estimation scheme and it detects large inputs of unknown magnitude by utilizing a decision tree and the Bayes decision rule. The impulsive input in the system equation corresponds to the existence of an edge of an obstacle. Fig. 6 shows modified

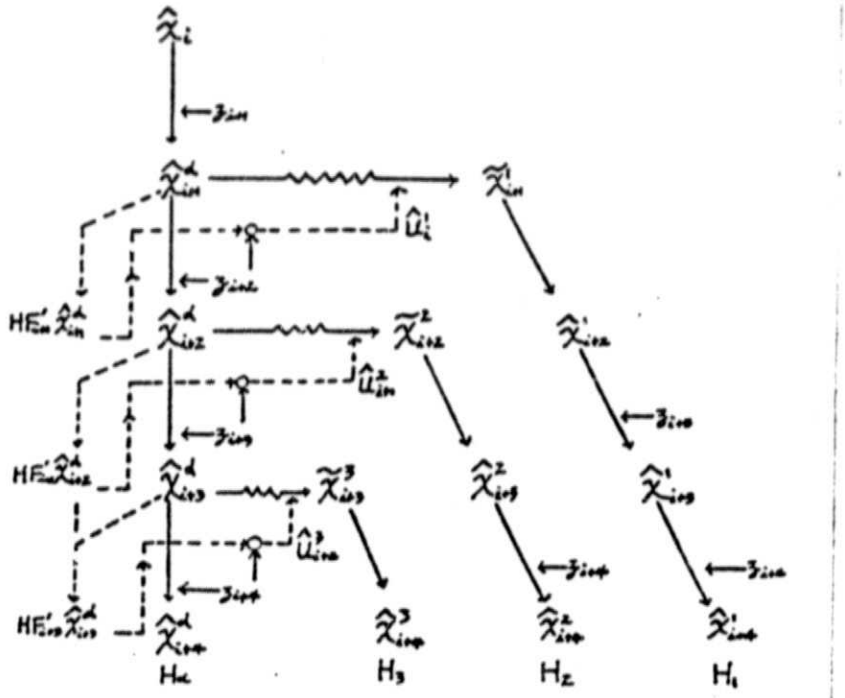

Fig. 6. Basic Decision Tree with Input Estimations.

ORIGINAL PAGE IS
OF POOR QUALITY

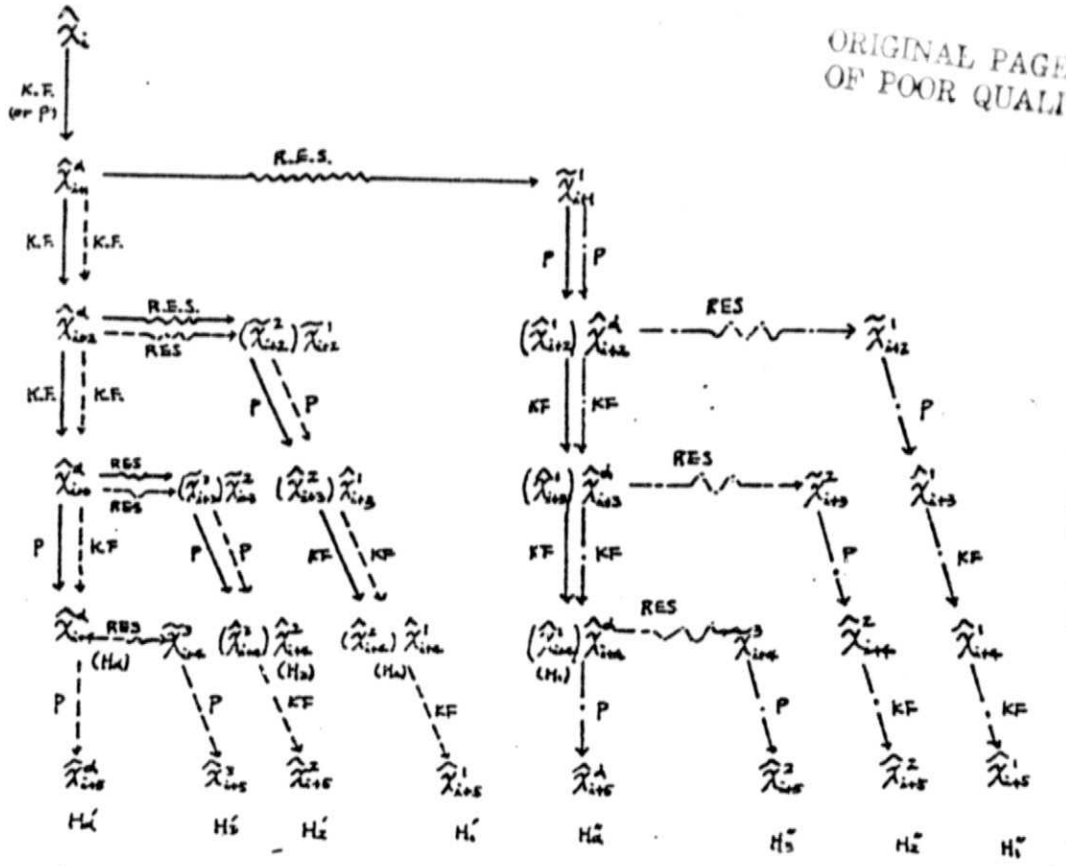

Fig. 7. Consecutive Decision Tree.

decision tree, each of which represents a particular hypothesis as follows:

H_1; impulsive input exists between stages i and i+1.

H_2; impulsive input exists between stages i+1 and i+2.

H_3; impulsive input exists between stages i+2 and i+3.

H_∂; no input exists between stages i and i+4.

With reference to Fig. 6, along branch α, the conditional state estimates $\hat{x}^{\alpha}_{i+2}$, $\hat{x}^{\alpha}_{i+3}$ and $\hat{x}^{\alpha}_{i+4}$ are obtained by using Kalman filter equations, since H_α assumes no impulsive input between stages i and i+4. The procedure to estimate the state at stage i+1, $\hat{x}^{\alpha}_{i+1}$, will be discussed later.

For branch 3, the state estimates for stages i+1 and i+2 are the same as branch α. Since H_3 assumes in input between stages i+2 and i+3, $\hat{x}^3_{i+3}$ is obtained by utilizing an input estimation scheme. As shown in Reference 2, the input estimation $\hat{u}^3_{i+2}$, is obtained from z_{i+4}, since the existence of an input u_{i+2} does not affect z_{i+3} but z_{i+4} directly. As a result, $\hat{x}^3_{i+3}$ is obtained by utilizing measurement data z_{i+4} one stage ahead. Since z_{i+4} has already been used for the estimation of $\hat{x}^3_{i+3}$, it cannot be used twice. Thus, the following stage estimate $\hat{x}^3_{i+4}$ is obtained by prediction only. As is noticed from above discussion, we need at least 4 stages to distinguish branch 3 from branch α.

For branch 2, the state estimate at stage i+1 is the same as $\hat{x}^{\alpha}_{i+1}$. However, the stage estimate $\hat{x}^2_{i+2}$ is obtained by using an input estimation scheme. This is because H_2 assumes an input between stages i+1 and i+2. As a consequence, $\hat{x}^2_{i+2}$ is estimated by using measurement data z_{i+3} one stage ahead. The following state $\hat{x}^3_{i+3}$ is estimated by prediction only, since z_{i+3} has already been used for the estimation of $\hat{x}^2_{i+2}$. To make branch 2 comparable with branch α and branch 3, stage estimate $\hat{x}^2_{i+4}$ is obtained by using an input estimation scheme, since H_1 assumes an input between stages i and i+1. The following state $\hat{x}^1_{i+2}$ is estimated by prediction only, since z_{i+2} has already been used for the estimation of $\hat{x}^1_{i+1}$. To make branch 1 to be comparable with the rest of the branches, state estimates $\hat{x}^1_{i+3}$ and $\hat{x}^1_{i+4}$ are obtained by Kalman filter equations which use the measurement data z_{i+3} and z_{i+4} respectively.

As shown in Fig. 7, which will be discussed later, the state estimate $\hat{x}^{\alpha}_{i+1}$ is obtained by either prediction or Kalman filtering. If the state $\hat{x}_i$ has been obtained by utilizing input estimation scheme in the former decision tree, $\hat{x}^{\alpha}_{i+1}$ is obtained by prediction only, since the data z_{i+1} has already been used in the former stage. On the other hand, if x_i is obtained by Kalman filtering in the former decision tree $\hat{x}^{\alpha}_{i+1}$ is obtained by using Kalman filtering. The conditional state estimates along the decision tree in Fig. 6 and the corresponding covariances are used for the computation of the joint conditional probability of the residues for each branch of the decision tree as follows:

$$\Pr(\overset{m}{r}_{i+1},\ r^m_{i+2},\ r^m_{i+3},\ r^m_{i+4} | x_i,\ H_m) \qquad \text{(a)}$$

$$r^m_{i+1} \triangleq z_{i+1} - E\{H\, x_{i+1} | x_i,\ H_m\} = z_{i+1} - H\, f_i'\, \hat{x}_i \quad \text{for } m = 1,2,3,\alpha \qquad \text{(b)}$$

$$r^m_{i+2} \triangleq z_{i+2} - E\{H\, x_{i+2} | \hat{x}^{\alpha}_{i+1} H_m\} = z_{i+2} - H\, f'_{i+1}\, x^{\alpha}_{i+1} \quad \text{for } m - 1,2,3\alpha \qquad \text{(c)}$$

$$r^m_{i+3} \triangleq z_{i+3} - E\{H\, x_{i+3} | \hat{x}^\alpha_{i+2}, H_m\} = z_{i+3} - H\, F'_{i+2}\, \hat{x}^\alpha_{i+2} \quad \text{for } m = 2,3\alpha \qquad (d)$$

$$r^1_{i+3} \triangleq z_{i+3} - E\{H\, x_{i+3} | \hat{x}^1_{i+2}, H_1\} = z_{i+3} - H\, F'_{i+2}\, \hat{x}^1_{i+2} \qquad (e)$$

$$r^m_{i+4} \triangleq z_{i+4} - E\{H\, x_{i+4} | \hat{x}^\alpha_{i+3}, H_m\} = z_{i+4} - H\, F'_{i+3}\, \hat{x}^\alpha_{i+3} \quad \text{for } m = 3,\alpha \qquad (f)$$

$$r^m_{i+4} \triangleq z_{i+4} - E\{H\, x_{i+4} | \hat{x}^m_{i+3}, H_m\} = z_{i+4} - H\, F'_{i+3}\, \hat{x}^m_{i+3} \quad \text{for } m = 1,2 \qquad (g)$$

The joint conditional probabilities are used to evaluate the Bayes risk index R_ℓ for the branch ℓ as defined below:

$$R_\ell = \sum_{m=1,2,3,\alpha} P_m C_{\ell m} P_r(r^m_{i+1}, r^m_{i+2}, r^m_{i+3}, r^m_{i+4} | x_i, H_m) \qquad (2)$$

where P_m; priori probability for H_m.

$C_{\ell m}$; cost associated with accepting H_ℓ when H_m is true.

If R_2, R_3 or R_α is minimum, it is concluded that there is no input between stages i and i+1. As a consequence, the state estimate $\hat{x}^\alpha_{i+1}$ is accepted as a correct state estimate and branch 1 is discarded. As shown in dotted line in Fig. 7, with $\hat{x}^\alpha_{i+1}$ as a new initial state, branches 2, 3 and α are extended to stage i+5 and become branches 1, 2 and α respectively. Branch 3 is newly generated and the algorithm proceeds with a new set of data.

If R_1 is minimum, it is concluded that there is an input between stages i and i+1. $\hat{x}^1_{i+1}$ is accepted as a correct estimate for stage i+1 and totally new set of decision tree is generated to the stage i+5 with $\hat{x}^1_{i+1}$ as a new initial state. This procedure is illustrated in chain dotted line in Fig. 7. It should be noted again that $\hat{x}^\alpha_{i+2}$ should be obtained by Kalman filter equations when $\hat{x}^\alpha_{i+1}$ is accepted as a correct state estimate. When $\hat{x}^1_{i+1}$ is accepted as a correct state estimate, $\hat{x}^\alpha_{i+2}$ is obtained by prediction only since the measurement data z_{i+2} has already been used for the estimation of $\hat{x}^1_{i+1}$ in the former decision tree.

Now, the joint conditional probability in equation (2) is computed as follows:

$$P_r(r^m_{i+1}, r^m_{i+2}, r^m_{i+3}, r^m_{i+4} | \hat{x}_i, H_m) = P_1(r^m_{i+4} | \hat{x}_i, z_{i+1}, z_{i+2}, z_{i+3}, H_m) \cdot$$

$$P_r(r_{i+3} | \hat{x}^m_i, z_m, z_{i+2}, H_m) \cdot P_r(r^m_{i+2} | \hat{x}_i, z_{i+1}, H_m) \cdot P_r(r^m_{i+1}\, \hat{x}_i, H_m) \qquad (3)$$

It should be pointed out that the last term of equation (12), $P_r(r^m_{i+1} | x_i, H_m)$ is the same for all branches, since r^m_{i+1} is common to all the branches as can be seen in the decision tree of Fig. 6. For this reason, reduced joint conditional probability $P_r(r^m_{i+2}, r^m_{i+3}, r^m_{i+4} | \hat{x}^\alpha_{i+1}, H_m$ will be used for comparison among the hypothesis.

As Markov property has been preserved in the procedure of state estimations, the reduced joint conditional probability for each branch is written as follows:

$$P_r(r^1_{i+2}, r^1_{i+3}, r^1_{i+4} | \hat{x}^{\alpha}_{i+1}, H_1) = P_r(r^1_{i+4} | \hat{x}^1_{i+3}, H_1) \cdot P_r(r^1_{i+3} | \hat{x}^1_{i+2}, H_1) \cdot P_r(r^1_{i+2} | \hat{x}^{\alpha}_{i+1}, H_1) \tag{4a}$$

$$P_r(r^2_{i+2}, r^2_{i+3}, r^2_{i+4} | \hat{x}^{\alpha}_{i+1}, H_2) = P_r(r^2_{i+4} | \hat{x}^2_{i+3}, H_2) \cdot P_r(r^2_{i+3} | \hat{x}^{\alpha}_{i+2}, H_2) \cdot P_r(r^{\alpha}_{i+2} | \hat{x}^{\alpha}_{i+1}, H_2) \tag{4b}$$

$$P_r(r^3_{i+2}, r^3_{i+3}, r^3_{i+4} | \hat{x}^{\alpha}_{i+1}, H_3) = P_r(r^3_{i+4} | \hat{x}^{\alpha}_{i+3}, H_3) \cdot P_r(r^{\alpha}_{i+3} | \hat{x}^{\alpha}_{i+2}, H_2) \cdot P_r(r^{\alpha}_{i+2} | \hat{x}^{\alpha}_{i+1}, H_3) \tag{4c}$$

$$P_r(r^{\alpha}_{i+2}, r^{\alpha}_{i+3}, r^{\alpha}_{i+4} | \hat{x}^{\alpha}_{i+1}, H_{\alpha}) = P_r(r^{\alpha}_{i+4} | \hat{x}^{\alpha}_{i+3}, H_{\alpha}) \cdot P_r(r^{\alpha}_{i+3} | \hat{x}^{\alpha}_{i+2}, H_{\alpha}) \cdot P_r(r^{\alpha}_{i+2} | \hat{x}^{\alpha}_{i+1}, H_{\alpha}) \tag{4d}$$

For the computation of $P_r(r^1_{i+2} | \hat{x}^{\alpha}_{i+1}, H_1)$ in equation (4a), the expected value of residue r^1_{i+2} is $HF^1_{i+1}Bu_i$ as shown in equation (6) of Reference 2. As a result, the correct evaluation of the probability would be:

$$P_r(r^1_{i+2} | \hat{x}^{\alpha}_{i+1}, H_1) = \frac{1}{\sqrt{2\pi |w^1_{i+2}|}} \text{Exp} \{ -\frac{1}{2} J^1_{i+2} \} \tag{5a}$$

where

$$J^1_{i+2} = \hat{r}^{1\,T}_{i+2}, w^{1\,-1}_{i+2}, \hat{r}^1_{i+2} \tag{5b}$$

$$w^1_{i+2} = \text{cov} \{ \hat{r}^1_{i+2} \}, \tag{5c}$$

and

$$\hat{r}^1_{i+2} = r^1_{i+2} - HF'_{i+1} Bu_i \tag{5d}$$

Since u_i in equation (5d) is unknown, the best approximation would be to substitute $HF'_{i+1}Bu^1_i$ by $HF'_{i+1}B\hat{u}^1_i$ which is derived in equation (c8) of Reference 2.

Thus, the residue $\hat{r}^1_{i+2}$ becomes:

$$r^1_{i+2} = r^1_{i+2} - HF'_{i+1} Bu_i = r_{i+2} - HF'_{i+1} Bu^1_i \equiv 0 \tag{5e}$$

Since the input estimate $\hat{u}^1_i$ is obtained from one shot estimation by using z_{i+2}, it does not distinguish noise from signal. This approximation will result in a deterministic quantity as shown in equation (5e), and exact evaluation of the probability $P_r(r^1_{i+2} | \hat{x}^{\alpha}_{i+1}, H_1)$ is not possible. It is found that similar problems occur with the evaluation of the probabilities $P_r(r^2_{i+3} | \hat{x}^{\alpha}_{i+2}, H_2)$, and $P_r(r^{\alpha}_{i+4} | x^{\alpha}_{i+3}, H_3)$ in equations (4b) and (4c) respectively. Thus, the j.c.p. for each branch becomes:

Branch 1: $P_r(r^1_{i+4}, r^1_{i+3} | \hat{x}^1_{i+2}, H_1) = P_r(r^1_{i+4} | \hat{x}^1_{i+3}, H_1) \cdot P_r(r^1_{i+3} | \hat{x}^1_{i+2}, H_1)$ (6a)

Branch 2: $P_r(r^2_{i+4}, r^\alpha_{i+2} | \hat{x}^\alpha_{i+1}, r^2_{i+3}, H_2) = P_r(r^2_{i+4} | \hat{x}^2_{i+3}, H_2) \cdot P_r(r^\alpha_{i+2} | \hat{x}^\alpha_{i+1}, H_2)$ (6b)

Branch 3: $P_r(r^\alpha_{i+3}, r^\alpha_{i+2} | \hat{x}^\alpha_{i+1}, H_3) = P_r(r^\alpha_{i+3} | \hat{x}^\alpha_{i+2}, H_3) \cdot P_r(r^\alpha_{i+2} | \hat{x}^\alpha_{i+1}, H_3)$ (6c)

For branch α, all the conditional probabilities in equation (4d) can be evaluated. Since the same number of probabilities are needed to be compared with other branches, only first two probabilities are chosen to be used.

Branch α: $P_r(r^\alpha_{i+3}, r^\alpha_{i+2} | \hat{x}^\alpha_{i+1}, H_\alpha) = P_r(r^\alpha_{i+3} | \hat{x}^\alpha_{i+2}, H_\alpha) \cdot P_r(r^\alpha_{i+2} | \hat{x}^\alpha_{i+1}, H_\alpha)$ (6d)

As is noticed in equations above, the estimation of the states $\hat{x}^\alpha_{i+4}$, $\hat{x}^3_{i+3}$ and $\hat{x}^3_{i+4}$ are not needed for the evaluation of the probabilities. In the procedure of redefining the j.c.p. of each branch as above, the j.c.p. of H_3 and H_α become the same, since the two hypotheses share the same branch till the stage i+3. As a result, branch 3 is deleted from the decision tree and the state estimate $\hat{x}^3_{i+4}$ in branch α is not needed. The final structure of the decision tree with the residues to be compared are illustrated in Fig. 8.

Now we can explain heuristically how the R.E.S. distinguishes a large input to the system from a large observation noise. For the purpose of explanation, assume the diagonal element of the cost matrix is zero and all others are equal. Also the priori probabilities for the branches are equal. It can be shown that this leads to a maximum likelihood decision rule for multiple hypotheses except that the R.E.S. proceeds one stage for each decision recursively. Since each of the probability functions is Gaussian, the one with smaller residue will have larger probability. One may analyze the effect of 5 cases on the residuals for the 3 branches. The 5 cases are:

1. A large impulse input u_i between stages i and i+1.
2. No input, but large observation noise v_{i+2} with z_{i+2}.
3. A large impulse input u_{i+1} between stages i+1 and i+2.
4. No input, but large observation noise v_{i+3} with z_{i+3}.
5. No input, but large observation noise v_{i+4} with z_{i+4}.

For case 1, there is an input between stages i and i+1; then $\hat{x}^1_{i+1}$ would be a correct estimate and the following residues r^1_{i+3} in equation (1e) and r^1_{i+4} in equation (1g) becomes small. On the other hand, $\hat{x}^\alpha_{i+1}$ which does not include input estimation of u_i, would be a wrong estimate. Large residues result in r^α_{i+2} in equation (1c) and r^α_{i+3} in equation (1d). For case 2, there is a large observation noise with z_{i+2}, then $\hat{x}^1_{i+1}$ includes a spurious input estimate which is not present and the following residuals r^1_{i+3} and r^1_{i+4} become large. On the other hand, $\hat{x}^\alpha_{i+1}$ is obtained by filtering the observation noise by Kalman filter and the following residuals r_{i+2} and r^α_{i+3} will be small. This line of reasoning leads to Table II which illustrates the qualitative picture of the residuals for the five cases mentioned above.

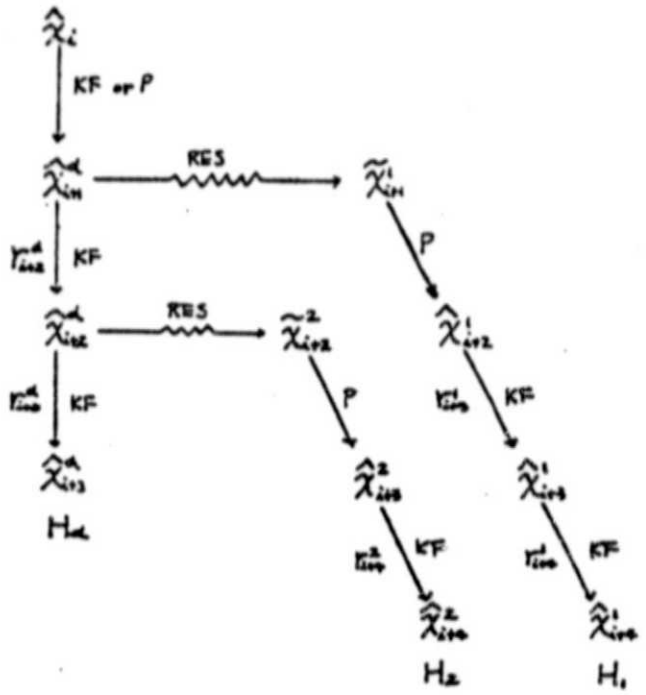

ORIGINAL PAGE IS
OF POOR QUALITY

Fig. 8. Final Structure of Decision Tree.

Fig. 9. Edge of Boulder (left) and Crater (right) at 50m, outlined by R.E.S.

Table II

	case 1 large u_i	case 2 large v_{i+2}	case 3 large u_{i+1}	case 4 large v_{i+3}	case 5 large $+4$
Branch 1 r^1_{i+3}	small	large	large	large	small
r^1_{i+4}	small	large	large	small	large
Branch 2 r^α_{i+2}	large	large	small	small	small
r^2_{i+4}	large	small	small	large	large
Branch r^α_{i+2}	large	large	small	small	small
r^α_{i+3}	large	small	large	large	small

Looking at Table II, one can notice that:

In case 1, branch 1 is likely to have the largest probability, and detect the presence of input.

In case 2, branch 1 will have the smallest probability and the scheme will succeed to ignore the measurement noise v_{i+2} and proceed to the next stage.

In case 3, branch 2 will have the largest probability. The scheme will proceed to the stage i+1 and detect the input afterwards.

In case 4, all the branches are equally likely, since all the branches have one large residue and one small residue.

In case 5, branch α is most likely, and the scheme will proceed to the next stage.

It has been shown qualitatively that R.E.S. would work very well except for case 4. Since all of the 3 branches are equally likely in case 4, a slight biasness in the cost assignment or priori probability will handle the situation.

Computer simulations were performed for a boulder-crater obstacle pair located 40m and 4m away from the rangefinder. Range data were obtained from a previously developed program which simulates the rangefinder measurements. The measurement data were corrupted by a Gaussian noise with its standard deviation 0.05m. The rangefinder was assumed to be located 2m above ground, and the boulders and craters were of hemispherical shape with 2m in diameter. For the cost matrix, the diagonal elements C_{11}, C_{22} and C_{33} are assigned the value zero, since correct decision should cost the least. All the off diagonal elements are set to 1.0, so that no excessive penalties are assigned to the false detections. In the simulation with obstacles at 40m, elevation angle β of the rangefinder changes from 0.7° to 3.3° with constant increment $\Delta\beta = 0.04^\circ$ and azimuth angle changes from -5° to 5° with $\Delta = 0.2^\circ$. The simulation result in Fig. 9 shows that the modified R.E.S. succeeded in reducing almost all the false detections without using excessive penalties to false detections. In the simulation with obstacles at 4m, β changes from 8.21° to 45.52° with

$\Delta\beta = 1.49^{o}$ and the azimuth angle θ changes from -45^{o} to 45^{o} with $\Delta\theta = 3.6^{o}$. Fig. 10 shows the outline of obstacles extracted by modified R.E.S. It is noted that the modified R.E.S. detected half of the bottom edges of the boulder at 4m which could not be detected by the previous R.E.S. Approximate signal to noise ratios at the edges of the obstacles were computed according to the formula $SNR = u/\sigma_m$, where u is the magnitude of the impulsive input occuring at the edge of obstacle and σ_m is the standard deviation of the noise. The SNR at the bottom of a boulder at 4m is found to be in the neighborhood of 1.4 while the SNR at the bottom of a boulder at 40m is about 7.0. This is the reason why the detection of the bottom edge of the boulder at 4m has been a harder task to be performed.

In summary, for the particular set of state equations and measurement equations that we considered, the existence of an input does not affect the next measurement but affects the measurement data after the next. For this reason, the first section of the decision tree becomes common to every branch, thus it is excluded from comparing the j.c.p. The magnitude of an input is estimated by second residue which is one shot estimation. This one shot estimation cannot distinguish the signal from noise. The conditional probability for the residues which include the input estimation becomes deterministic and these probabilities are deleted from comparing the j.c.p. for the branches. To test whether the R.E.S. can distinguish a large itput from a large noise, the residues of the branches are compared qualitatively as a measure in determining where the decision scheme is correct.

In conclusion, the stabilized R.E.S. with modified decision tree generated only few false detections in identifying the complete outlines of obstacles without using excessive penalties to the false detections. Also, with the reinforced detection ability, R.E.S. detected half of the bottom edges of the boulder at 4m.

Thus far, R.E.S. assumed that each column or row of the range matrix is independent and ignored the interdependency between each other. It is thought that the detection ability of the R.E.S. will be increased if R.E.S. is expanded to incorporate the interdependency between the columns and rows.

TASK C. Integrated Path Selection System for Martian Rover Using Laser Rangefinder - C. S. Kim
Faculty Advisor: Prof. C. N. Shen

There have been separate studies on obstacle detection, References 1, 2, terrain modeling and evaluation, References 3, 4, and path selection algorithms, References 4, 6. With the introduction of the logarithmic scanning scheme and obstacle identification scheme, an overall performance of the integrated path selection system for autonomous Martian rover is demonstrated in this work.

With reference to Fig. 11, a laser rangefinder is used to obtain the measurement data. A logarithmic scanning scheme is designed so that it can provide the obstacle detection and terrain modeling algorithms with a set of measurement data meaningful in the sense of data spacing over the entire scanning area. The design of the scanning scheme becomes complicated due to the noise elements in the range as well as in the positioning angles. By processing the range measurement data obtained, Rapid Estimation Scheme, Reference 2, detects the possible edges of the discrete obstacles. The result of R.E.S. is fed into an identification scheme in which the whole set of detected points are classified into subsets. Each subset is recognized either as a boulder, a crater, or a ridge. Now, the location and sizes of the obstacles

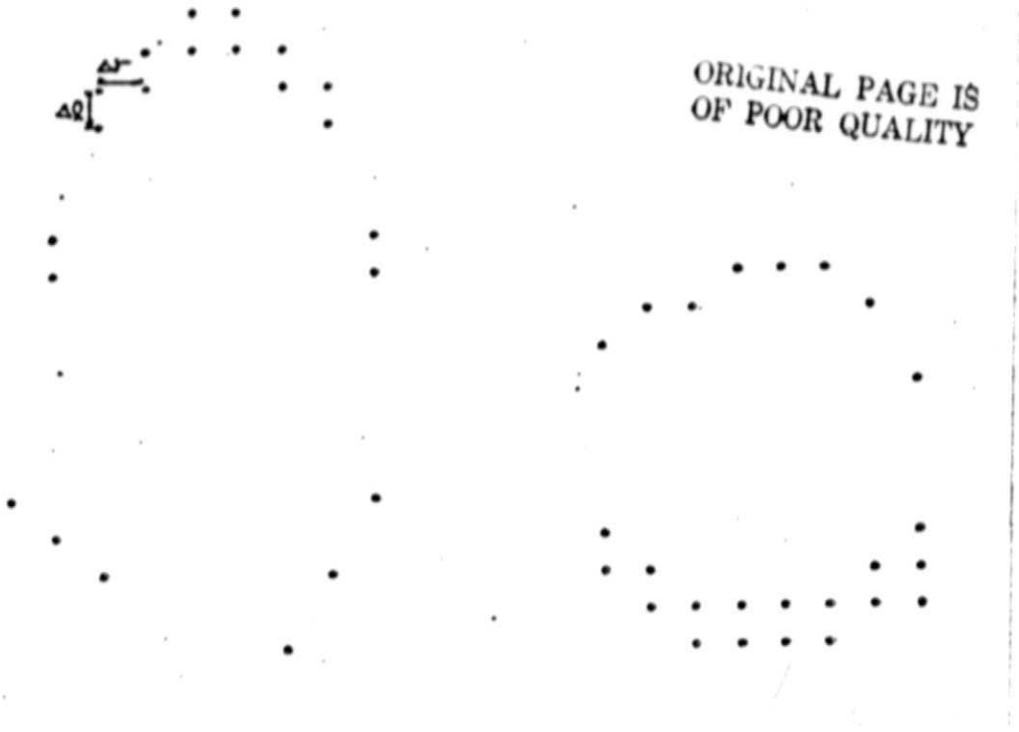

ORIGINAL PAGE IS
OF POOR QUALITY

Fig. 10. Edge of Boulder (left) and Crater (right) at 5m, outlined by R.E.S.

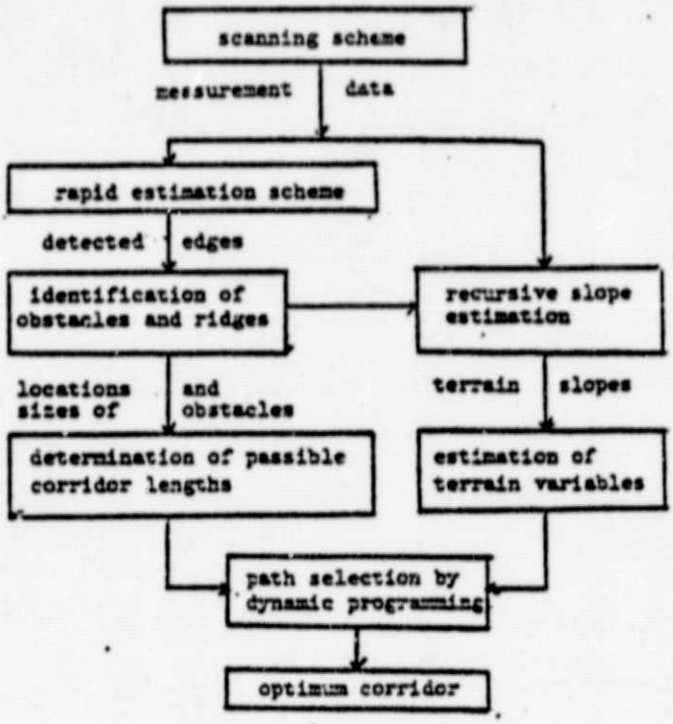

Fig. 11. Block Diagram of Path Selection System.

ORIGINAL PAGE IS
OF POOR QUALITY

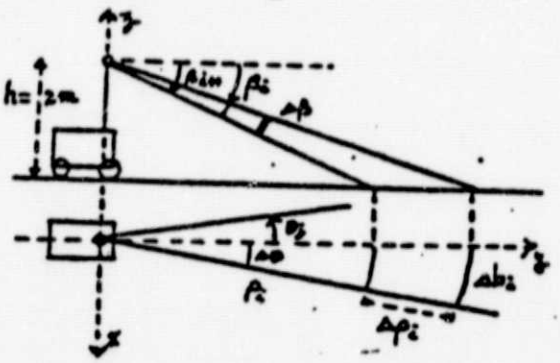

Fig. 12. Coordinate System.

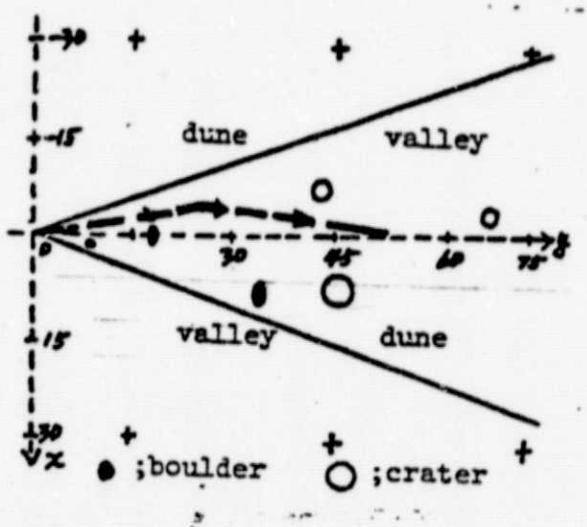

Fig. 13. Terrain Model used in Simulation.

are used to determine the lengths of the passable corridors for the path selection scheme. In parallel with the R.E.S., the inpath and cross-path slopes at the data points are estimated by recursive slope estimation scheme, Reference 4. This recursive algorithm is not valid at the edges of obstacles and ridges where discrete changes in range occur. Since the edges of obstacles and ridges are known from the obstacle detection scheme, the slope estimation scheme will initialize itself at those points. Inpath and cross-path slopes computed at the data points are utilized to estimate the terrain variables at the spine and track points along each corridor. The terrain variables considered are inpath slope, tilt slope, wheel deviation and body clearance. Since the spine or track points do not coincide with the measurement data points, the inpath slopes, cross-path slopes and elevations at the spine and track points are estimated from two-dimensional Hermite interpolation function, Reference 8, in a rectangular coordinate system. Now, each corridor is evaluated in terms of the terrain variables. The corridor which is expected to incur the least amount of energy consumption and risk is chosen by dynamic programming method as the optimum corridor in the path selection scheme.

The range measurement data is obtained by changing the elevation angle β_i and azimuth angle θ_j in spherical coordinate system. The three coordinate systems used in this work are depicted in Fig. 12:

spherical coordinate - (ℓ, θ, β)

cylindrical coordinate - (ρ, θ, Z)

rectangular coordinate - (x, y, z)

It is desired for the scanning scheme to cover a horizontal terrain from 5m to 80m in radial direction from the rangefinder 2m in height. The resolution of the rangefinder is limited by the noise elements in positioning angles as well as the range error. It is assumed that the standard deviations of the elevation angle and the measurement range are σ_β=1 arc-minute and σ_m = 0.05m respectively. Scanning scheme is evaluated by three criteria as follow:

(i) signal to noise ratio of the incremental elevation angle, $\Delta\beta_i/\sigma_{\Delta\beta}$;

(ii) horizontal data spacing in radial direction, $\Delta\rho_i$;

(iii) signal to noise ratio of the incremental range, $\Delta m_i/\sigma_{\Delta m}$.

Assuming that β_i's and m_i's have Gaussian distribution, the quantities $\sigma_{\Delta\beta}$ and $\sigma_{\Delta m}$ become:

$$\sigma_{\Delta\beta} = N\bar{2}\ \sigma_\beta = 1.414 \text{ arc-min.}$$

$$\sigma_\Delta = N\bar{2}\ \sigma_m = 0.07\text{m}$$

It is noticed that to have $\Delta\beta_i/\sigma_{\Delta\beta}$ and $\Delta m_i/\sigma_\beta$ greater than unity, the corresponding $\Delta\beta_i$ and Δm_i should be greater than 1.414 arc-minutes and 0.07m respectively all over the scanning area. Since the obstacle detection scheme needs at least four data points, inside or on the obstacle to be identified, the horizontal data spacing $\Delta\rho_i$ determines the size of obstacles that can be identified. If constant increment of radial distance $\Delta\rho$ = 0.5m is used, the

the obstacle detection scheme can detect obstacles of 2m in size for all range. However, $\Delta\beta_i$ becomes smaller at far distances and at ρ_i = 80m, $\Delta\beta_i$ becomes 0.54 arc-min., which is much smaller than its standard deviation $\sigma_{\Delta\beta}$ = 1.414 arc-min. Even if constant increment of radial distance $\Delta\rho_i = \Delta\rho$ = 1.82m will result in the incremental elevation angle $\Delta\beta_i$ = 2 arc-min. at ρ_i = 80m, the obstacle detection scheme cannot identify obstacles whose dimensions are less than 7m in size.

To design a scanning scheme which will make $\Delta\rho_i$ at near distance as small as possible while keeping $\Delta\beta_i/\sigma_{\Delta\beta}$ and $\Delta m_i/\sigma_{\Delta m}$ greater than unity, the following variable increment of elevation angle is suggested. With reference to Fig. 12, the relation between $\Delta\rho_i$ and $\Delta\beta_i$ is derived as follows:

$$2\Delta\beta_i h/\sin 2\beta_i = \Delta\rho_i \tan\beta_i \qquad (1)$$

where $0<\beta_i<\pi/2$ and $0<\Delta\beta_i$ and h is the height of the rangefinder.

If the quantity $\Delta\rho_i \tan\beta_i$ in equation (1) is set to a constant, $\Delta\rho_i$ becomes smaller and $\sigma\beta_i$ becomes larger as β_i gets larger. From this reasoning, the scanning scheme will result in a large data spacing at far and smaller data spacing at near distances. By setting the radial data spacing $\Delta\rho_i$ to equal the horizontal data spacing $\Delta\beta_i$, it has been derived in Reference 7 that the quantity $\Delta\rho_i$ becomes smaller logarithmically as the index i increases. In Table III, the resulting data spacings and the corresponding incremental elevation angles are listed.

Table III

Data Spacing and Signal to Noise Ratios

ρ_i	80m	50m	25m	5m
$\Delta\rho_i = \Delta\beta_i$	2.4m	1.5m	0.75m	0.15m
$\Delta m_i/\sigma_{\Delta m}$	34.3	21.4	10.7	2.1
$\Delta\beta_i$	2.7 arc-min.	4.3 arc-min.	8.4 arc-min.	36.5 arc-min.
$\Delta\beta_i/\sigma_{\Delta\beta}$	1.9	3.0	5.9	25.8

From the measurement data obtained in this manner, R.E.S. can identify the obstacles whose dimensions are as small as 0.6m at ρ_i = 5m and dimension of 6m at ρ_i = 50m. The range data obtained according to this logarithmic scanning scheme are stored in the form of range matrix

$$M = \begin{bmatrix} M_{11} & M_{12} & \cdots & M_{1n} \\ M_{21} & M_{22} & \cdots & M_{2n} \\ \vdots & & & \\ M_{k1} & M_{k2} & \cdots & M_{kn} \end{bmatrix} \qquad (2)$$

To cover a sector in horizontal remain defined by $5m \leq \rho \leq 80m$ and $-0.54 \text{ rad} \leq \theta \leq 0.54 \text{ rad}$, the required number of rows and columns of the range matrix in equation (2) are k = 102 and n = 37 respectively.

Now, R.E.S., Reference 2, processes the measurement data obtained from logarithmic scanning scheme to detect the possible edges of obstacles. To show the detection ability of the R.E.S., range measurement data are obtained from a previously developed range measurement simulation program. The general terrain model is a wavy surface with plateaus and valleys analytically defined in rectangular coordinate system as:

$$z = 0.5 \cos\left(\frac{\pi y}{30}\right) \sin\left(\frac{\pi x}{30}\right) \tag{3a}$$

where the units of x, y and z are meters. Also the following features are super-imposed on the general terrain described by equation (3a)

(i) hemi-ellipsoidal boulders at (x, y) = (0,17) and (11,34);

(ii) hemi-spherical boulder at (x, y) = (1,7);

(iii) hemi-spherical craters at (x, y) = (7,45), (-9,44), and (-4,67).

The top view of this terrain is shown in Fig. 13. The rangefinder is located at (x, y, z) = (0,0,2) and the scanned area is defined by $S_{max} = 0.3805$ rad, $\beta_{min} = 0.025$ rad, $\theta_{max} = 0.54$ rad, and $\theta_{min} = -0.54$ rad. In the process of generating the measurement data, white Gaussian noise with 0.05m standard deviation is added to each of the range measurements.

The measurement data obtained are processed by R.E.S. The vertical edges of the boulders, crater and ridges are detected as '*', and the side edges are detected as '0' in Fig. 14. In Fig. 15, top of the ridges are identified by chains of several column detections. Boulders are identified by consecutive column detections at the top and single column detections at the bottom. Craters are identified by single column detections at far edges and consecutive column detections at near edges. It should be noted that the use of R.E.S. is subject to produce false detections as well as to miss some of the detections.

As has been mentioned previously, it is needed to develop a scheme which will identify the whole set of detection points into subsets of detections. By utilizing the characteristics of the boulder, crater and ridge, as well as the required relationship between the detected points to form an outline of an obstacle, an algorithm has been developed, Reference 7, to identify a set of detections as a boulder, a crater or a ridge. By using the identification scheme, the whole set of detection points obtained from R.E.S. in Fig. 14 is characterized either as a boulder, a crater, a ridge or a false detection. As shown in Fig. 15, the scheme clearly identified each of the boulders, craters and the ridges. This information is fed into path selection scheme in determining the lengths of the passable corridors.

Recursive slope estimation scheme, Reference 4, was developed earlier to estimate the inpath and cross-path slopes at the data points by utilizing the range data. As has been mentioned earlier, this scheme cannot be applied where discrete jump in range occurs, such as edges of obstacles and ridges. Since the edges of obstacles and ridges are identified by R.E.S. and obstacle identification scheme, the recursive slope estimation scheme is modified to reinitialize itself at those points. For simulation of the scheme, the range

ORIGINAL PAGE IS
OF POOR QUALITY

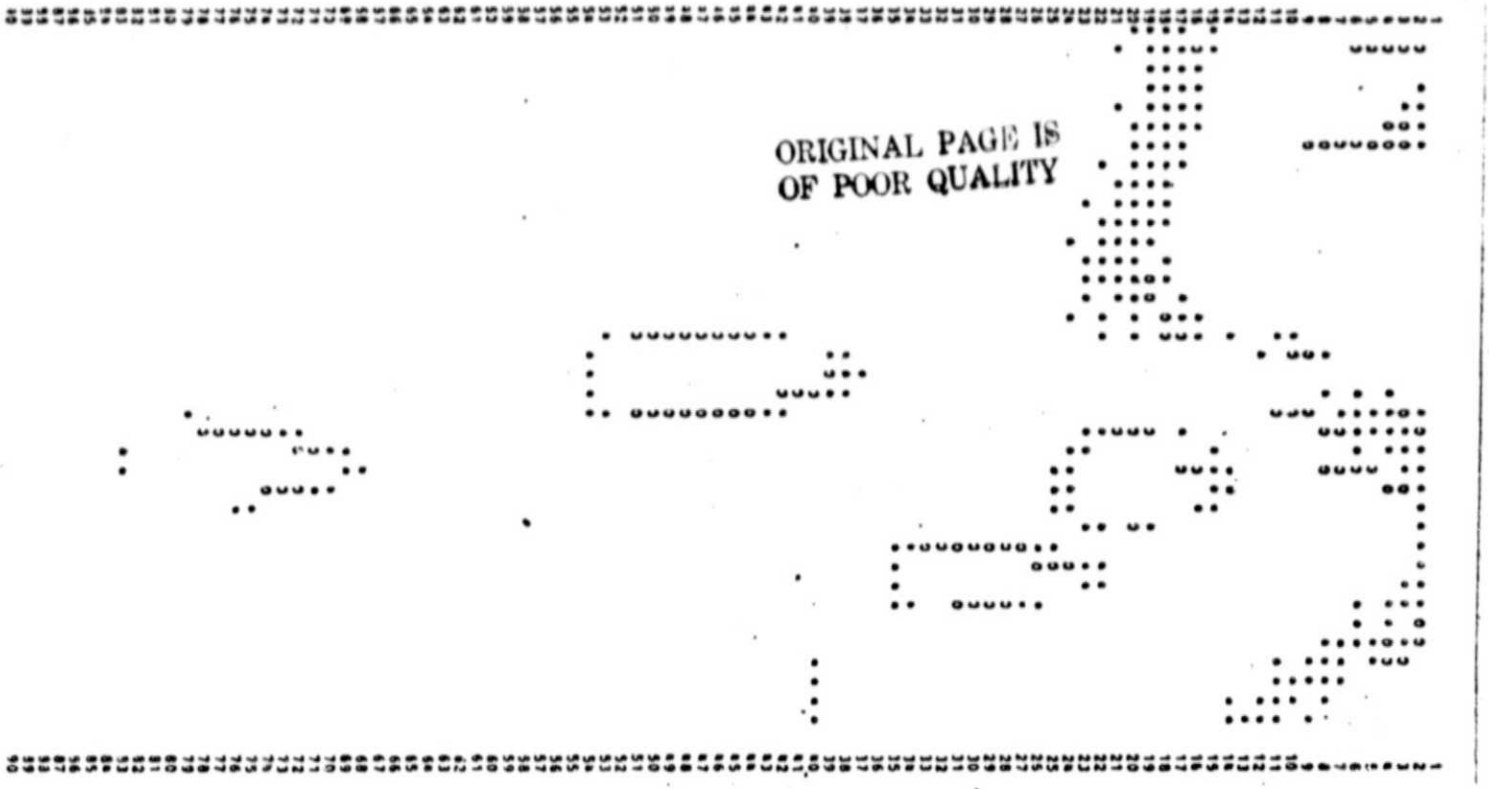

Fig. 14. Detected Edges by R.E.S.

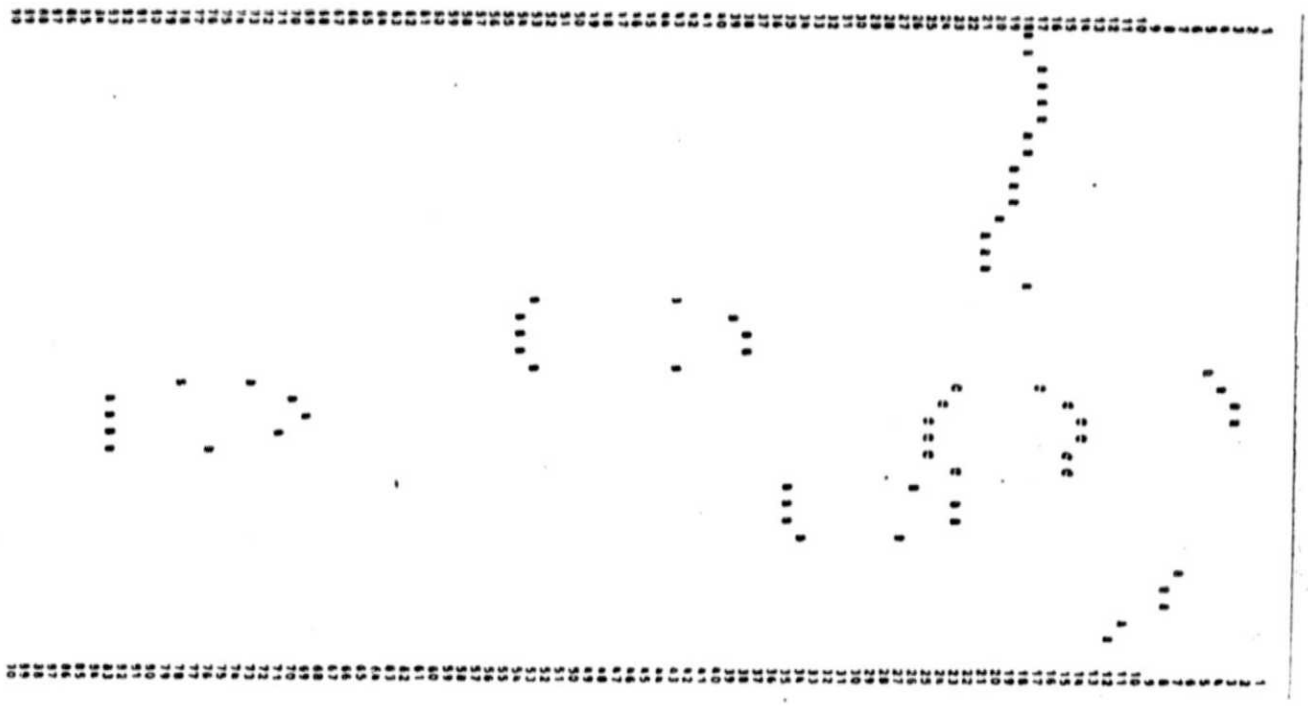

Fig. 15. Outlines of Obstacles and Ridges.

data obtained for the terrain in Fig. 13 are processed by the recursive slope estimation scheme. To display the information, the gradient for each data point is classified to lie within a specified interval for mapping purpose. Each interval and the corresponding character is defined in Table IV.

Table IV

Isogradient Regions

Character	Gradient min	Gradient max
A	0.0	0.02
B	0.02	0.04
C	0.04	0.06
D	0.06	0.08
E	0.08	0.1
F	0.1	0.15
G	0.15	0.2
H	0.2	0.3
I	0.3	0.4
J	0.4	∞
U	undefined	gradient

Fig. 16 shows as isogradient map describing the terrain in x-6 plane projection. It is noted that there are circular isogradient regions on the faces of sinusoidal dunes and valleys. Also, high gradients such as 'J' are assigned on the faces of boulders and inside the crater. It is also noted that hidden regions exist at the back of a boulder or inside the crater where laser beam could not reach. Undefined gradient, represented by character 'u', occurs when the recursive algorithm cannot be applied due to a large discrete change in ranges between the adjacent measurement data. The estimated inpath and cross-path terrain slopes and the iso-gradient map are used for the evaluation of the passable corridors.

So far, we have obtained the outlines of obstacles and slope estimates at the data points by utilizing logarithmic scanning scheme, R.E.S., obstacle identification scheme, and recursive slope estimation scheme. Now, with the information obtained above, path selection scheme is utilized to determine an optimal corridor which minimizes certain performance indexes. The path selection scheme used here is based on the method outlined in the previous work, References 5, 6. One major modification made to the previous work is the evaluation of terrain variables. Since we have already obtained the slopes at the data points, the terrain variables (inpath slope, tilt slope, body clearance and wheel deviation) are estimated by employing two-dimensional Herminte interpolation function which utilizes the estimated terrain slopes. A detailed description of the modifications is found in Reference 7. The simulation of the path selection procedure was performed for the terrain illustrated in Fig. 13. With the starting location (x, y) = (0,0) and the target location (0,350), the rover determines the corridor lengths and evaluates the terrain variables by utilizing the algorithms described earlier. Finally, optimum corridor is chosen by path selection scheme. The cost associated with each corridor is tabulated in Fig. 17 where the index (i, j) corresponds to that of the primary corridor CR_i and secondary corridor CR_{ij}. The length of primary corridors CR_3 and CR_4 become short due to the presence of obstacles

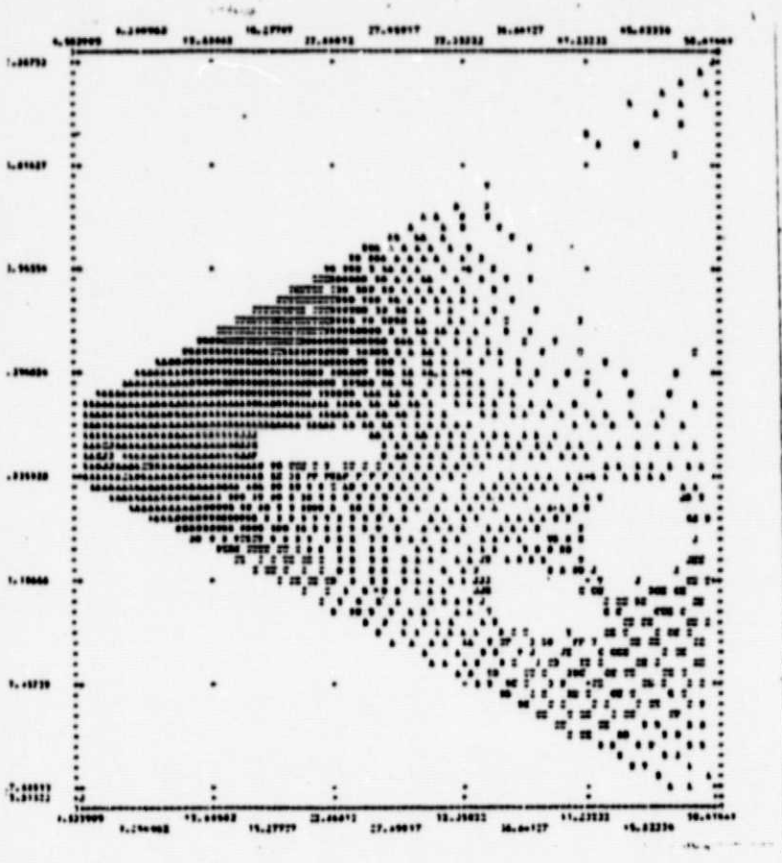

Fig. 16. Isogradient Map.

MEAN = 0.0 THETA = 0.0

(I,J)	PRIMARY COST	SECONDARY COST	TERMINAL	TOTAL COST
(1,1)	1.3102	0.3906	1.6359	3.3663
(1,2)	1.3102	0.3952	1.6359	3.3609
(1,3)	1.3102	0.6195	1.6359	3.5692
(1,4)	1.3102	0.8204	1.6359	3.7661
(1,5)	1.3102	1.2362	1.6359	4.1819
(2,1)	0.7462	9.7166	1.6861	12.0669
(2,2)	0.7462	0.3606	1.6861	2.9188
(2,3)	0.7462	0.5779	1.6861	2.9281
(2,4)	0.7462	2.1990	1.6861	4.5463
(2,5)	0.7462	7.1576	1.6861	9.5078
(3,1)	100.0000	1.3716	100.0000	201.3716
(3,2)	100.0000	100.0000	100.0000	300.0000
(3,3)	100.0000	100.0000	100.0000	300.0000
(3,4)	100.0000	100.0000	100.0000	300.0000
(3,5)	100.0000	1.1061	100.0000	201.1061
(4,1)	100.0000	1.2292	100.0000	201.2292
(4,2)	100.0000	0.2663	100.0000	200.2663
(4,3)	100.0000	100.0000	100.0000	300.0000
(4,4)	100.0000	100.0000	100.0000	300.0000
(4,5)	100.0000	1.6695	100.0000	201.6695
(5,1)	1.5872	1.4819	1.7890	4.8581
(5,2)	1.5872	0.3450	1.7890	3.7212
(5,3)	1.5872	100.0000	1.7890	103.3762
(5,4)	1.5872	100.0000	1.7890	103.3762
(5,5)	1.5872	100.0000	1.7890	103.3762

OPTIMAL PATH IS 25.000 METERS IN THE DIRECTION THETA = -0.10

THE CORRESPONDING COST IS 2.3109 FOR THE CORRIDORS (2,2)

Fig. 17. Corridor Costs.

ORIGINAL PAGE IS
OF POOR QUALITY

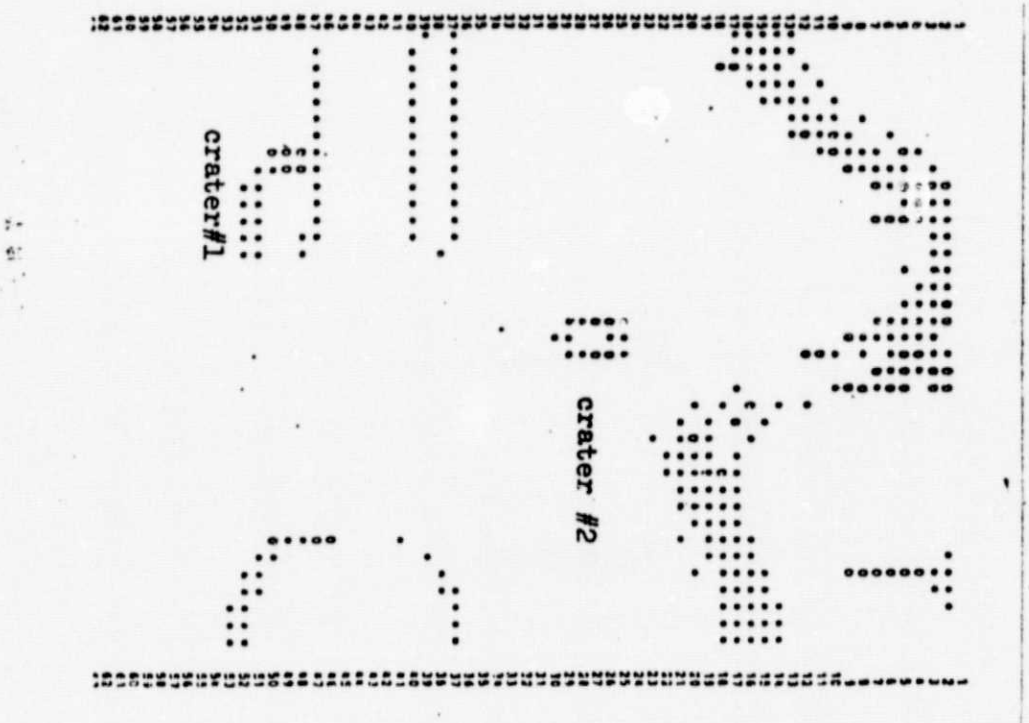

Fig. 18. Detected Edges at (x, y) = (4.5, 24.6)

at near distances. The value 100 is assigned to penalize short corridors. The terminal costs for CR_1 and CR_5 become larger because of the target deviation and low elevation at the end of the corridor. As is noted in Fig. 17, the scheme selected the corridor of 25m in the direction $\theta = 0.18$ rad for the corridors (2,2). In the next path selection procedure, the rover scans the terrain at the position (x, y) = (-4.5, 24.6). The measured data are processed by R.E.S. to detect the possible edges of obstacles. Fig. 18 shows the outlines of craters detected. Crater #1 corresponds to the crater at (x, y) = (-9,44), which was not detected in the first path selection because it was hidden by the ridge. Crater #2 corresponds to the crater at (x, y) = (-4,67). It was not detected in the first path selection procedure since it is too small compared to the data spacing at the far distance. Now, the rover utilizes again the terrain evaluation and path selection scheme described earlier. In this second path selection procedure, the corridor of 25m in the direction $\theta = 0.18$ rad is selected as optimum corridor. The route resulting from the two path selection procedure is illustrated in dotted line in Fig. 13.

In conclusion, this work presents an integrated study of logarithmic scanning, obstacle detection, terrain evaluation, and route designation problem. The resolution provided by the scanning scheme is appropriate for the detection of small obstacles at near distances as well as large obstacles at far. The outline of obstacles and ridges are identified from the detected points. This information is used in the design of passable corridors in that the corridor lengths become adaptive to the obstacles identified. The terrain variables along each corridor are computed by using the terrain slopes estimated recursively. The path selection procedure is made more practical by employing a finite dimension vehicle rather than a point mass. The integrated system for the autonomous navigation of Mars rover is completed by establishing the coordinations among existing algorithms as well as making modifications to them. Computer simulation results are promising in that the rover is capable of selecting a locally optimum path for low risk and energy expenditure while maintaining a desired target direction.

The following are the areas in which more research work is needed for improved performance of the route designation problem for autonomous Mars rover:

(i) Adaptive scanning scheme.
It is needed to develop a scheme which will detect the skyline and make the scanning scheme adaptive to the upgraded hills as well as downgraded valleys.

(ii) Improvement on the obstacle identification scheme.
The obstacle identification scheme outlined in Reference 7 is just a beginning of the contour extraction problem. A more rigorous study is needed to employ all the possible information in constructing the outlines of the obstacles and ridges.

(iii) Improvement on path selection scheme.
In the previous path selection scheme, Reference 5, all the terrain variables computed are treated in a deterministic manner. It is needed to modify the previous scheme so that the stochastic nature of the terrain variables are considered in the evaluation of the cost for each corridor.
Also, in the previous scheme, the relation between the probability of impassability and the amount of risk involved is not clear.

REFERENCES

(1) Sonalker, R.V. and Shen, C.N., "Mars Obstacle Detection by Rapid Estimation Scheme from Noisy Laser Rangefinder Readings," Proceedings of the Milwaukee Symposium on Automatic Computation and Controls, Wisconsin, April 1975, pp. 291-296.

(2) Kim, C.S., Marynowski, R.C. and Shen, C.N., "Obstacle Detection Using Stabilized Rapid Estimation Scheme with Modified Decision Tree," Proceedings of JACC, October 1978.

(3) Shen, C.N. and Stare, J.G., "Estimation of Terrain Iso-Gradient from a Stochastic Range Data Measurement Matrix," Proceedings of JACC, San Francisco, California, June 1977.

(4) Pawlowski, P.R., "Recursive Computation Structures and Two-Dimensional Interpolation for Terrain Iso-Gradient Estimation from Stochastic Range Data," Master's Project, R.P.I., 1978.

(5) Netch, A. and Shen, C.N., "Terrain Evaluation and Route Designation Based on Noisy Rangefinder Data," Proceedings of the 7th Annual Pittsburgh Conference on Modeling and Simulation, University of Pittsburgh, Pennsylvania, April 1977.

(6) Ring, H. and Shen, C.N., "Path Selection Process Utilizing Rapid Estimation Scheme," Proceedings of the 9th Annual Pittsburgh Conference on Modeling and Simulation, University of Pittsburgh, Pennsylvania, April 1978.

(7) Shen, C.N. and Kim, C.S., "A Laser Rangefinder Path Selection System for Martian Rover using Logarithmic Scanning Scheme," to be presented in VIII IIAC Symposium on Automatic Control in Space, Oxford, United Kingdom, 1979.

(8) Mitchell, A.R. and Wait, R., "Finite Element Method in Partial Differential Equations," John Wiley & Sons, 1977, pp. 64-73.

(9) Shen, C.N. and Yerazunis, S.W., "Data Acquisition and Path Selection Decision Making for an Autonomous Roving Vehicle," R.P.I. Technical Report MP-60, Progress Report for January-July 1978, pp. 13-23.